Supplementary information for

Spiral microchannel with rectangular and trapezoidal cross-sections for size based particle separation

Guofeng Guan,[a,b] Lidan Wu,[c] Ali Asgar Bhagat,[b†] Zirui Li,[b,d] Peter C Y Chen,[a,b] Shuzhe Chao,[a] Chong Jin Ong,[a] and Jongyoon Han,[*b,c,e]

[a] *Department of Mechanical Engineering, National University of Singapore, Singapore*

[b] *Biosystems and Micromechanics IRG, Singapore-MIT Alliance for Research and Technology (SMART), Singapore*

[c] *Department of Biological Engineering, Massachusetts Institute of Technology, USA*

[d] *College of Mechanical and Electrical Engineering, Wenzhou University, China*

[e] *Department of Electrical Engineering and Computer Science, Massachusetts Institute of Technology, USA*

[†] *Present Address – Clearbridge Biomedics Pte Ltd, Singapore*

Force balance analysis of particle in curved channel

A particle flowing with surrounding fluid is subject to the following known forces: the Drag force $\mathbf{F_D}$, the centrifugal force $\mathbf{F_C}$, the buoyancy force, *i.e.* the pressure gradient force $\mathbf{F_B}$, two unsteady forces due to a change of the relative velocity, the added mass force or virtual mass force $\mathbf{F_A}$, and the Basset History force $\mathbf{F_H}$, the gravitational force $\mathbf{F_G}$, and the inertial lift force $\mathbf{F_L}$.

We will now discuss each of these forces applied on the suspended particles in the inertial flow regime.

***(i)* Drag force $\mathbf{F_D}$** – The drag force on the particle is in the direction of relative flow velocity $\mathbf{U}_r$ with respect to the particle. The magnitude of $\mathbf{F_D}$ can be given as

$$\mathbf{F_D} = \frac{1}{2}\pi\rho_f r^2 \mathrm{C_D}\mathbf{U}_r^2$$

where $\mathrm{C_D}$ is the drag coefficient, ρ_f is the density of fluid, and r is the radius of particle. In a curved channel with secondary flow, $\mathbf{U}_r$ is a combination of two perpendicular relative flow velocities: the slip velocity $\mathbf{U}_s$ along the main flow, which is refer to the velocity difference between particle and fluid along x direction, and the Dean velocity $\mathbf{U_D}$ for a particle focused at a balanced point in the channel's cross section. Thus we have $\mathbf{U}_r = \mathbf{U}_s + \mathbf{U}_\mathrm{D}$ as shown in Figure 1A.

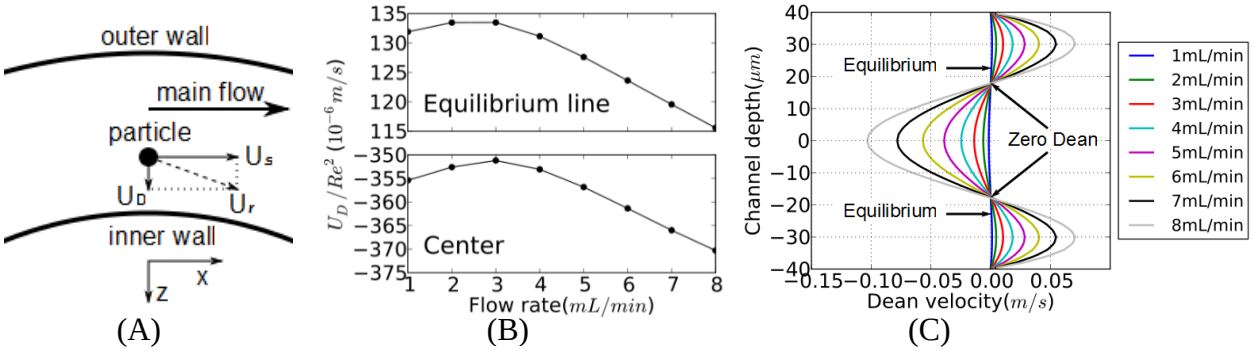

Figure 1. (A) Schematic illustrates the relative flow velocity around a particle from top view of a curved channel**. (B)** The trend of Dean velocity $\mathbf{U_D}$ increases with Re according to simulation in a rectangular channel. The value of $\mathbf{U_D}$ in the top curve is the magnitude of Dean velocity at 22% of channel depth (focusing position), while $\mathbf{U_D}$ in the bottom curve is the value of Dean velocity at center of channel. **(C)** Magnitude of Dean velocity along y-axis at different flow rate at center line of channel width.

According to Yang's simulation[1], in a tube Poiseuille flow with a freely rotating particle of a radius $r =$

0.075D at equilibrium position under moderate Reynolds number $\mathrm{Re} = \frac{8\rho_f r^2 \mathbf{U_m}}{\mu D}$, where $\mathbf{U_m}$ is the mean velocity of the main flow in the channel, D is the hydraulic diameter of the tube (equivalent to the depth of channel here), and μ is the dynamic viscosity of the fluid, the flow velocity of particle $\mathbf{U_p}$ is smaller than that of the surrounding fluid $\mathbf{U_f}$. The slip velocity is given by $\mathbf{U_s} = \mathbf{U_f} - \mathbf{U_p} = \frac{0.0412\mathrm{Re}^{1.04}\mu}{2r\rho_f} \approx 0.05\,\mathbf{U_m}$.

For a given point, $\mathbf{U_D}$, according to our simulation result of an 80 μm deep 600 μm wide rectangular cross section channel, is generally proportional to Re^2, *i.e.* the magnitude of $\mathbf{U}_m^2$, which is different from Ookawara's result of $\mathbf{U_D} \sim \mathbf{U}_m^{1.63}$.[2] The disagreement might be due to the difference of structural parameters between the two models. From Figure 1B&C, it can be seen that Dean flow velocity increases slightly faster than $\sim\mathbf{U}_m^2$ when the flow rate is less than 3mL/min, both at the center and at 22% of channel (near the minimum lift force plane (Figure 6 of main article), where particles are focused). On the other hand, $\mathbf{U_D}$ increases more slowly than $\mathbf{U}_m^2$ (approximately ~ $\mathbf{U}_m^{1.8}$) at flow rate >4.0mL/min. The maximum magnitude of $\mathbf{U_D}$ achieved in the system is $0.037\mathbf{U_m}$, which is at the flow rate of 8.0mL/min ($\mathbf{U_m}$ = 2.778m/s).

In our system, for flow rates from 1.0 to 8.0 mL/min, we have the Reynolds number of the particle $0.26 < \mathrm{Re}_p = \frac{2\rho_f r \mathbf{U_r}}{\mu} < 2.59$ calculated based on the above analysis of $\mathbf{U_r}$. Based on Morsi's[3] analysis/model, the C_D for $0.1 < \mathrm{Re}_p < 1.0$ and $1.0 < \mathrm{Re}_p < 10.0$, could be estimated by equation $C_D = \frac{22.73}{\mathrm{Re}_p} + \frac{0.0903}{\mathrm{Re}_p^2} + 3.69$ and $C_D = \frac{29.1667}{\mathrm{Re}_p} - \frac{3.8889}{\mathrm{Re}_p^2} + 1.22$, respectively. Here, to simplify the analysis, we take the first-order approximation, $C_D = \frac{24}{\mathrm{Re}_p}$, which will make the calculated $\mathbf{F_D}$ slightly smaller than the actual value. The drag force then follows Stokes Law as $\mathbf{F_D} = \frac{1}{2}\pi\rho_f r^2 \frac{24}{\mathrm{Re}_p}\mathbf{U}_r^2 = 6\pi\mu r\mathbf{U_r}$. The component of $\mathbf{F_D}$ induced by the Dean flow in the channel's cross section is thus given by

$$\mathbf{F_{DD}} = 6\pi\mu r\mathbf{U}_D$$

Although there is shear in the Dean flow and the particle will rotate according to both the shear of the main flow and the Dean flow in the channel, Kurose[4] demonstrated that the shear rate and rotation velocity caused by the Dean flow do not have significant effect on the direction and magnitude of the drag force at Re_p in above range. The Dean induced drag $\mathbf{F_{DD}}$ is thus should be always along the Dean direction and is proportional to the local Dean velocity $\mathbf{U_D}$.

***(ii)* Lift force $\mathbf{F_L}$** – Sinc $\mathbf{U_D}$ is two orders of magnitude smaller than $\mathbf{U_m}$ in the curved channel, here we only consider the lift force induced by the main flow. The lift force comes from two separate effects: the slip-shear of the fluid surrounding the particle, which is first identified by Saffman[5], and the slip rotation of the particle in fluid, known as Magnus effect[4]. The distribution of $\mathbf{F_L}$ in a square cross-section straight channel was studied others, however no mathematical calculations were given[6]. Here, to show the relationship between $\mathbf{F_L}$ and the flow velocity as well as the particle diameter, the lift force equation of a freely rotating particle in steady flow within a cylindrical tube by Yang[1] is used. In a tube Poiseuille flow with a freely rotating particle of radius $r = 0.075D$ near the equilibrium position,

$$\mathbf{F_L} = 1.085\mathrm{Re}^{1.064}\mu r\mathbf{U}_s\left(\frac{\omega_d}{\omega_e} - 1\right) \approx \frac{8.68\rho_f r^3 \mathbf{U}_m \mathbf{U}_s}{D}\left(\frac{\omega_d}{\omega_e} - 1\right)$$

where D is the (hydraulic) diameter of tube, ω_d and ω_e are the slip angular velocities of the particle at a position with relative distance d from the center of the tube's cross section and equilibrium position respectively. The term ω_d/ω_e is a function of particle position d and Reynolds number Re

$$\frac{\omega_d}{\omega_e} = 0.00913\mathrm{e}^{9.2d}\mathrm{Re}^{1.08-2.1d}$$

$\mathbf{F_L}$ is zero at the equilibrium position, which is around 20% of D from the wall[7,8], and changes its direction when the particle move across the equilibrium position. The magnitude of $\mathbf{F_L}$ near the equilibrium position, according to above equations, is approximately proportional to $\mathbf{U_m U_s} \sim 0.05\mathbf{U_m^2}$.

(*iii*) Centrifugal force $\mathbf{F_C}$ – For a particle flowing in a curved channel with the radius of curvature R, the centrifugal force subjected to the particle is pointing towards the outer side of the channel along z direction and is proportional to $\mathbf{U_p^2}$:

$$\mathbf{F_C} = -\frac{m_p \mathbf{U_p^2}}{R},$$

where $m_p = \rho_p V_p = \frac{4}{3}\rho_p \pi r^3$ is the mass of particle. ρ_p and V_p represent the density and volume of particle respectively.

(*iv*) Buoyancy force $\mathbf{F_B}$ – In a fluid with constant pressure gradient, particles are subjected to a buoyancy force pointing to the center of the channel curvature, *i.e.* along z-axis direction,

$$\mathbf{F_B} = \rho_f a_f V_p,$$

where $a_f = \frac{\mathbf{U_f^2}}{R}$ is the centripetal acceleration of fluid around the particle. The force is opposite to $\mathbf{F_C}$ and proportional to $\mathbf{U_f^2}$.

(*v*) Added mass force $\mathbf{F_A}$ – If $\mathbf{U_f} \neq \mathbf{U_p}$, the centripetal acceleration or deceleration of particles must displace some volume of surrounding fluid as it moves through it, since the object and fluid cannot occupy the same physical space simultaneously. The particle can thus be considered to have an added mass. This added mass subjects the particles to an additional force since the particle and surrounding fluid are under different centrifugal velocity. This force points towards the outer side of the channel *i.e.* opposite to z-axis, given by

$$\mathbf{F_A} = -m_A(a_f - a_p) = \frac{1}{2}\rho_f V_p \frac{\mathbf{U_p^2} - \mathbf{U_f^2}}{R}.$$

(*vi*) Basset history force $\mathbf{F_H}$ – The Basset force describes the force due to the lagging boundary layer development with changing relative velocity (acceleration) of bodies moving through a fluid[9,10]. It is difficult to calculate accurately and is commonly neglected for practical reasons.

(*vii*) Gravitational force $\mathbf{F_G}$ – Gravity is at least one order smaller than centrifugal force in our case. It can be neglected here.

The resultant force acting on the particle in the yz plane (cross section of the channel), neglecting the smaller terms ($\mathbf{F_G}$, $\mathbf{F_H}$),

$$m_p \frac{\mathrm{d}\mathbf{U_p}}{\mathrm{d}t} = \mathbf{F_{DD}} + \mathbf{F_L} + \mathbf{F_C} + \mathbf{F_B} + \mathbf{F_A}$$

If we assume $\rho_p = \rho_f = \rho$, then we have

$$\mathbf{F_{ABC}} = \mathbf{F_C} + \mathbf{F_B} + \mathbf{F_A} = \frac{2\pi\rho r^3(\mathbf{U_f^2} - \mathbf{U_p^2})}{3R} \approx \frac{4\pi\rho r^3 \mathbf{U_f U_s}}{3R}$$

The resultant force $\mathbf{F_{ABC}}$ is pointing to the center of the channel curvature, and the magnitude is proportional to $\mathbf{U_f U_s}$, i.e. proportional to $\mathbf{U_m^2}$. It is one or two order smaller than $\mathbf{F_{DD}}$, as shown in Figure 2. The effect of $\mathbf{F_{ABC}}$ on the focus position is thus not dominant.

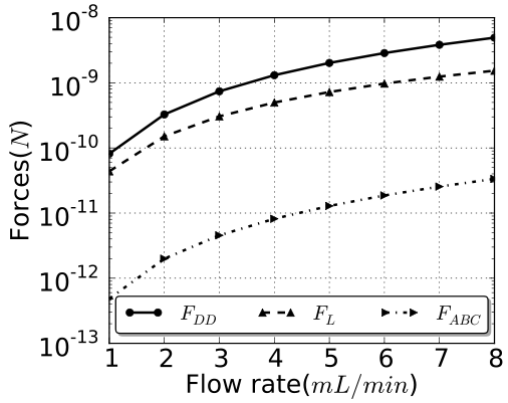

Figure 2 Magnitude of 3 major forces on a 15.5μm particle. $\mathbf{F_{DD}}$ and $\mathbf{F_{ABC}}$ are calculated based on the simulation of rectangular cross section channel, the particle is placed at the equilibrium position (22% of channel depth). $\mathbf{F_L}$ is calculated following Yang's simulation[1], and the direction is along the axial direction of cylindrical tube.

The effect of geometry of channel cross-section

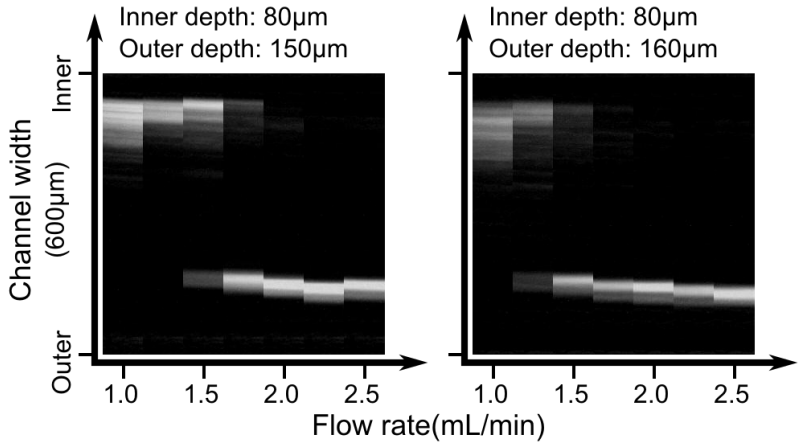

Figure 3 Effect of slant angle on particle focusing in trapezoidal cross-section spiral microfluidic channel. The white band in the image indicating the focus band of 15.5 μm fluorescent beads from the top view.

For a trapezoidal channel with a higher outer wall, there are many factors affecting the focusing position and separation efficiency, such as the width, inner and outer depth of the channel cross section, the radius of the spiral curvature, and the slant angle. As analyzed in the main article, the slant of the channel affects the focusing behavior in two ways: (i) at lower inner side, the increase of channel depth breaks the balance of the lift and drag force at high flow rate resulting in particle migration to the outer side and trapped at the vortex core, *i.e.* determines the threshold flow rate; and (ii) the location of the Dean vortex core. A large slant angle will lead to strong Dean at the outer side and increase trapping capability of particle. Large slant angle can also decrease the flow rate to drag out particles from the

inner side. Particles will switch to outer side at lower flow rate for large slant angle channel, which is confirmed by experiment observation in Figure 3 as well as the observation in Figure 3 of the main article.

As another validation of our understanding, three different channel cross-section geometries are fabricated and tested (Figure 4): normal trapezoidal cross section with constant slant angle, top wall convex cross section that have a large slant angle at the inner side but a small slant angle at the outer side, and a concave cross section with only the outer half having large slant angle.

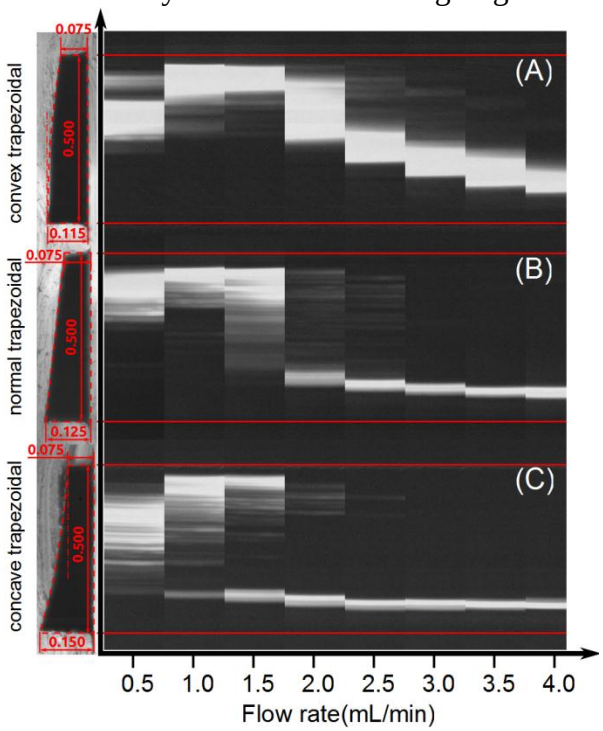

Figure 4 Top view microscopy images of 15.5μm fluorescent particles focus band shift with flow rate under different geometry of channel cross section. The width of the channel is 500μm. The inner depth is 75μm. Area of channel cross section is designed equally with all of three channels, $5.0\times10^{-2}mm^2$. Red lines indicate the channel wall. (A) Convex trapezoidal cross section. (B) Normal trapezoidal cross section. (C) Concave trapezoidal cross section.

For Convex slant channel (Figure 4A), the increase of depth mostly occurs at the inner side. Focused particle streams move to the outer side gradually with the increase of flow rate. Only a small shift occurs at 2mL/min, and stops at the middle of channel, where the slant angle decreases. In general, the performance of convex slant channel is closer to that of a rectangular cross section channel, and shares the same drawback of narrow physical separation between streams of different particle sizes when utilized for separation.

For concave slant channel (Figure 4C), the increase of channel depth mostly occurs at the outer side. Therefore, it generates strong Dean vortices even at lower flow rate. These strong Dean vortices are able to trap particles at much lower flow rate, compared with the normal slant channel (Figure 4B). On the other hand, since the slant angle is small, particles continue to remain focused at the inner side, generating two semi-stable focusing positions around 1 mL/min flow rate. In this situation, particles are separated into two bands at both sides of channel, which is also not desirable for particle separation.

Beside convex and concave trapezoidal channels, we have also tested spiral channels with varying top

wall geometries – stepped profile and a square wave. Other geometries such as high aspect ratio rectangular channel with H/W=15 and circular channel (by rolling a Tygon tubing) were also tested. None of them showed good performance in particle focusing and are hence not discussed and pursued further.

Video

Video S1: Top view of a separation between 18.68μm and 26.9μm particles at 3.4mL/min flow rate with an 80μm inner depth 130μm outer depth, 600μm wide spiral microchannel. Video was taken under Olympus X81(Olympus Inc., USA) microscope equipped with a high speed camera (Phantom V9.1, Vision Research Inc. USA). The optical lens of microscope is 10X. The exposure time for each frame is 4μs and the sample rate of the video is 2900pps.

References

1. Yang, B. H. *et al.* Migration of a sphere in tube flow. *Journal of Fluid Mechanics* **540**, 109–131 (2005).

2. Ookawara, S., Higashi, R., Street, D. & Ogawa, K. Feasibility study on concentration of slurry and classification of contained particles by microchannel. *Chemical Engineering Journal* **101**, 171–178 (2004).

3. Morsi, S. A. & Alexander, A. J. An investigation of particle trajectories in two-phase flow systems. *Journal of Fluid Mechanics* **55**, 193–208 (2006).

4. Kurose, R. & Komori, S. Drag and lift forces on a rotating sphere in a linear shear flow. *Journal of Fluid Mechanics* **384**, 183–206 (1999).

5. Saffman, P. G. The lift on a small sphere in a slow shear flow. *Journal of Fluid Mechanics* **22**, 385–400 (1965).

6. Di Carlo, D., Edd, J., Humphry, K., Stone, H. & Toner, M. Particle Segregation and Dynamics in Confined Flows. *Physical Review Letters* **102**, 1–4 (2009).

7. Schongerg A. Jeffrey & E.J., H. Inertial migration of a sphere in Poiseuille flow. *Journal of Fluid Mechanics* **203**, 517–525 (1989).

8. Nieuwstadt, H. A, Seda, R., Li, D. S., Fowlkes, J. B. & Bull, J. L. Microfluidic particle sorting utilizing inertial lift force. *Biomedical microdevices* **13**, 97–105 (2011).

9. Vojir, D. & Michaelides, E. Effect of the history term on the motion of rigid spheres in a viscous fluid. *International journal of multiphase flow* **20**, 547–556 (1994).

10. Coimbra, C. F. M. & Rangel, R. H. General solution of the particle momentum equation in unsteady Stokes flows. *Journal of Fluid Mechanics* **370**, 53–72 (1998).